International Journal of Microwave and Wireless Technologies, 2012, 4(6), 623–628. © Cambridge University Press and the European Microwave Association, 2012
doi:10.1017/S1759078712000608

RESEARCH PAPER

Wide aperture circularly polarized antenna for small telemetry satellites

M. KOUBEISSI[1], E. ARNAUD[1], M. THEVENOT[1], T. MONEDIERE[1], E. PERAGIN[2] AND H. DIEZ[2]

This paper focuses on the design of a telemetry antenna system intended for small satellites. It provides an axial ratio (AR) lower than 3 dB over ±60° conical space angle with over 20% of bandwidth. The antenna consists of a multilayer patch element fed by a wideband feeding circuit. The latter is an appropriate adjustment of 90° hybrid couplers and 180° ring coupler. We show that this design provides high-quality circular polarization properties for agile small satellites without having to suspend their mission to download their data and also without sacrificing the antenna low profile and wide bandwidth. The antenna is fabricated and the experimental performance is presented and followed by a discussion.

Keywords: Wide angle, Wide band, Circularly polarized antennas, Lightweight antennas, Small telemetry satellites

Received 12 March 2012; Revised 1 August 2012; first published online 19 September 2012

I. INTRODUCTION

In 1997, CNES (the National French Space Centre) started the development of a new high-performance and low-cost S-band TT&C transceiver for small platforms. Till date, more than 40 flight models have been delivered for diverse missions such as Rosetta, Deep Impact, and other CNES missions of the Microsat family.

In continuation to the development of the S-band transceiver, 4 years ago CNES started evaluating the potentiality of using COTS (Commercial Off-the-Shelf) satellite control software in X-band equipments.

The X-band transmitter under development is high-performance equipment especially designed and optimized for the needs and constraints of small platforms for which small volume, low mass, low power consumption, and low cost are important parameters.

There are currently various antenna systems (beam-scanning antennas and mechanically switched antennas) that allow agile satellite telemetry to download their data during the hearing phases or photo acquisition, but these devices are not suitable for small platforms due to their size, complexity or costs. Usually, when a standard antenna solution is used, observation tasks have to be interrupted in order to download telemetry data. The objective of this system is to provide a radio frequency link between the satellite and ground stations, regardless of the satellite latitude.

An innovative system which allows downloading telemetry in the presence of pitch and rolling platform movements has been invented by CNES [1]. The system is based on "active" and "distributed" antenna cells installed on several satellite sides and properly adjusted to provide the entire earth's coverage. A system of five cells allows covering ±60° pitch and roll. Hence, the aim of our work is to provide high quality circular polarized antenna over ±60° conical space angle around the antenna axis without scarifying the antenna low profile and wide bandwidth.

In fact, many articles [2–5] have concentrated on bandwidth widening techniques for microstrip antennas, there have been less concerns for optimizing their polarization quality as they get farther away from the boresight direction.

The paper presents the antenna design which is able to fit at best the wide aperture constraint.

It should be stressed here that the system is intended to operate in X-band, but for design validation purposes, the antenna is first designed for the WiFi band in order to make realization easier. The goal was to show the validity of the new design which is able to provide a wide aperture of circular polarization. Even if the frequency scaling is not a linear problem, a lower frequency design overcomes the mechanical fabrication problems. By a scaled design, we have validated the RF concept as well as the used technology. We now have a good knowledge about the expected results and difficulties that may be encountered during the fabrication process. Indeed, the thickness of the substrate is difficult to be precisely scaled and this task will be treated during design optimization.

Moreover, this antenna system is not limited for use in nano-satellites but in practice could be used for a number of communication applications. It should also be noted that the 2.4–2.48 GHz frequency band can be used for a data link application between nano-satellites.

II. ANTENNA DESIGN

The structure of this antenna is shown in Fig. 1. It is mainly made up of four substrate layers which support the feeding

[1]XLIM – CNRS 123, Avenue Albert Thomas, 87060, Limoges Cedex, France
[2]CNES –18 av. E. Belin, BPI: 3602, 31401, Toulouse Cedex 9, France
Corresponding author:
E. Arnaud
Email: Eric.arnaud@xlim.fr

https://doi.org/10.1017/S1759078712000608 Published online by Cambridge University Press

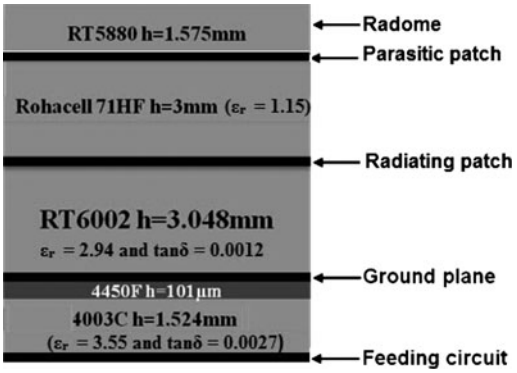

Fig. 1. The multilayer assembly and the conductor layers (side view).

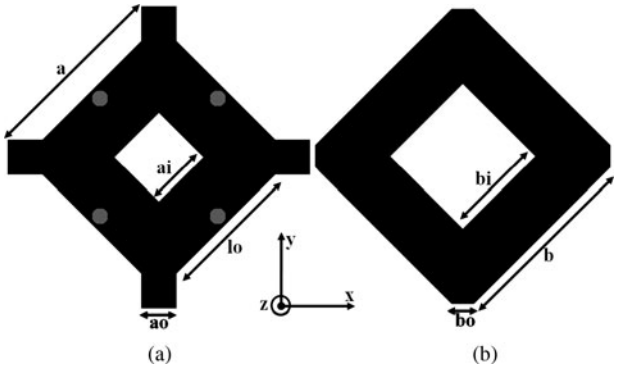

Fig. 2. Geometries of the main patch (a) and the parasite patch (b). (Dimensions are in mm: $a = 30$, $ai = 10$, $ao = 5.5$, $\mathrm{lo} = 22.2$, $b = 31.05$, $bi = 16.5$, $bo = 3.5$).

circuit, the main patch, the parasitic patch, and the radome. The patches are all squares and notched (truncated) whereas the ground plane is an 11-cm-radius disk. Patch excitations are made thanks to metallic cylindrical vias.

In order to enhance the antenna bandwidth, a passive parasitic patch is added to introduce a further resonance frequency [3, 4]. This parasitic patch is printed on the bottom side of an RT5880 substrate ($\varepsilon_r = 2.2$ and $\tan\delta = 0.0009$) whereas the metallization of the front side of the substrate is entirely removed, thus the radome is set up. Keep in mind that the substrates have low dielectric constants. As far as scan circular polarization is concerned, five techniques have been used to improve it over a wide angular scan.

- Four feed points with 90° sequential phase shift are used to feed the main patch.
- A square slot is etched in the center of the main patch, so the latter becomes a ring square patch.
- Four truncations are applied to the main and parasitic patches in order to improve the circular polarization quality in the operating band.
- The parasitic patch can be rotated by 45° compared with the main one in order to give a supplementary symmetrical structure or radiation in some cut planes. In fact, this rotation improves AR performance in certain cut planes but unfortunately, it decreases performance in the other orthogonally cut planes.
- The distance between the two patches and also the radius of the feeding probes are optimized and then the frequency bandwidth is increased with respect to a dual fed single patch.
- All these techniques lead to the radiating element structure shown in Fig. 2.

The gray points on the main patch in Fig. 2 present the feeding positions.

It should be noted that the inner and outer dimensions of the patches influence the bandwidth and the axial ratio (AR) quality. Hence, the dimensions must reach an agreement and the final values are obtained due to an optimization.

III. FEEDING CIRCUIT DESIGN

The feeding circuit is made up of two (3 dB, 90°) hybrid couplers and one 180° hybrid ring coupler as shown in Fig. 3. Indeed, modified three-branch couplers are used instead of two-branch hybrid coupler, in order to limit magnitude ripples and then improve the feeding circuit bandwidth. The aim of this circuit would be producing a 90° sequential phase shift over the whole desired frequency band with unbalanced magnitudes in order to contribute to a wide bandwidth of circular polarization.

This circuit has one 50 Ω input port (1) and four 50 Ω output ports (2–5). Since each hybrid coupler has two input ports there will then be two unused ports in the feeding circuit (6 and 7). The two unused ports (6 and 7) of the feeding circuit are loaded by quasi-50 Ω impedance. It should be noted that several bent lines have been added to the circuit design in order to avoid line crossovers and to reach a 90° sequential phase shift. As for the simulation results of the feeding circuit, the reflection coefficient remains below −15 dB over the (2.2–2.9 GHz) frequency bandwidth. The transmission S-parameters are shown in Fig. 4, where less than 0.5 dB magnitude balance is observed over (2.2–2.65 GHz) or 18% of frequency bandwidth.

Fig. 5 shows the phase shift between two adjacent output ports. Phase balances are about ±2° over 18% of frequency bandwidth.

The S-parameters of the feeding circuit are attractive and they lead to a wide frequency bandwidth. The feeding circuit is mounted below the ground plane of the antenna thanks to a bonding film in order to avoid parasitic radiations.

These simulation results cannot be verified by measurements due to feeding circuit design and the termination line location is away from the ground plane edges.

Moreover, we note that the circuit is chosen to be made up of different kind of couplers in order to obtain very good weightings at outputs. This is the reason why the feeding

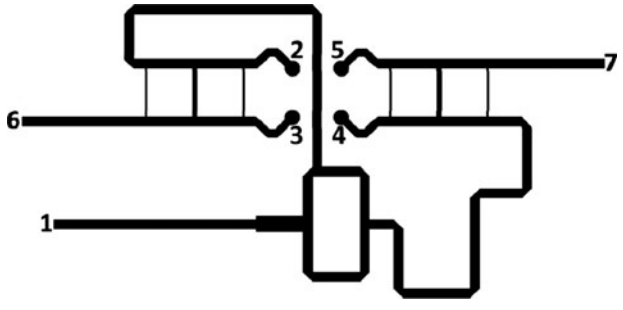

Fig. 3. Layout of the feeding circuit with the numbered ports.

https://doi.org/10.1017/S1759078712000608 Published online by Cambridge University Press

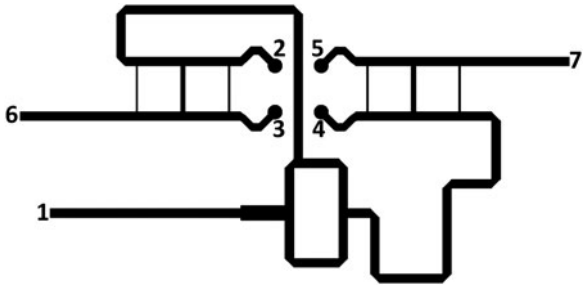

Fig. 4. Transmission S-parameters magnitude of the feeding circuit.

circuit is wide. It should be noted that the feeding circuits have naturally a wider operating bandwidth than the patch and then this later outweighs the whole design bandwidth.

The feeding circuit can be reduced by using a two-branch line instead of three-branch line hybrid coupler and a T power divider instead of ring coupler.

IV. ANTENNA PERFORMANCE

A) Design and fabrication procedure

The 3D antenna model has been simulated thanks to CST Microwave studio. As for the design, the feeding circuit and the main patch are printed on their substrates and assembled in a multilayer circuit thanks to 4450F bounding film. Next, the parasitic patch is printed on the bottom side of the RT5880 substrate where the demetallized front side is considered as radome. Hence, the antenna was realized by lithography procedure and was mounted on an aluminum support allowing the soldering of connectors and also structural rigidity. SMA connectors were welded to ports 1, 6, and 7. Finally, the multilayer (4003C–RT6002), Rohacell 71HF, and the RT5880 were manually assembled and tested. Pictures of the realized antenna are shown in Fig. 6. During the measurement series, 50 Ω loads are plugged to ports 6 and 7. The experimental results are given in sections B, C and D.

B) Electrical performance

The antenna's reflection coefficient is shown in Fig. 7. The simulated and measured −10 dB impedance definition bandwidth are about 800 MHz and 300 MHz, respectively. Even though there is a shape discrepancy between the simulated and realized reflection coefficient, the antenna remains matched over 300 MHz. It should be noted that patches resonances cannot be observed on the reflection coefficient plot. In fact, the feeding circuit masks the impedance bandwidth of the two patches.

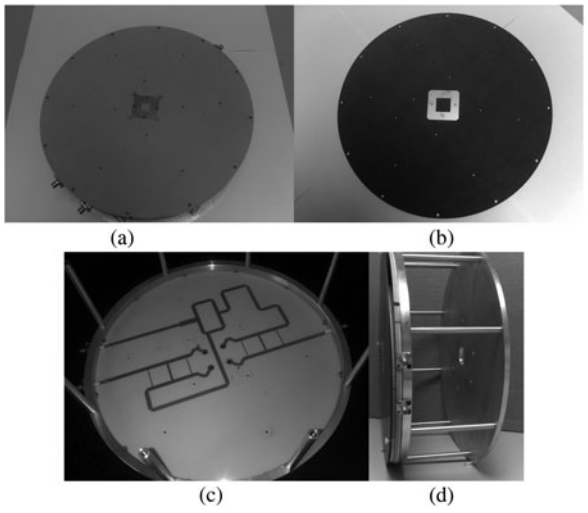

Fig. 6. Photography of the realized antenna. (a) RT6002 front view: main patch, (b) RT5880 bottom view: parasite patch, (c) 4003 C bottom view: feeding circuit, (d) antenna side view showing the metal holding structure and 2 SMA connectors.

C) Axial ratio

The boresight AR of the antenna is measured based on the frequency and is shown in Fig. 8.

It can be seen from Fig. 8 that the measured broadside AR remains below 3 dB over 300 MHz of frequency bandwidth, which means a correct circular polarization (CP). Unfortunately, the experimental CP bandwidth is lower compared with the simulated one (40%). Several refined simulations have been carried out and they prove that the air gap around the two sides of the Rohacell 71HF layer and the curvature of the RT5880 layer lead to performance deterioration and frequency shift. Indeed, acting on the distance between the main patch and the parasitic patch affects the resonance frequency of each one and thus the operating bandwidth.

Moreover, uncertainly substrates permittivities create inappropriate weightings at the output feeding circuit. A difference between the simulated and experimental results of

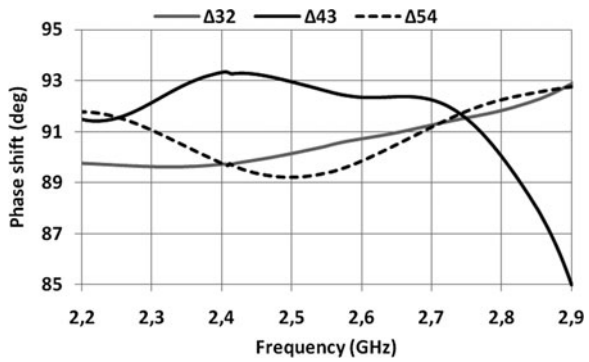

Fig. 5. Phase shift at the output ports of the feeding circuit.

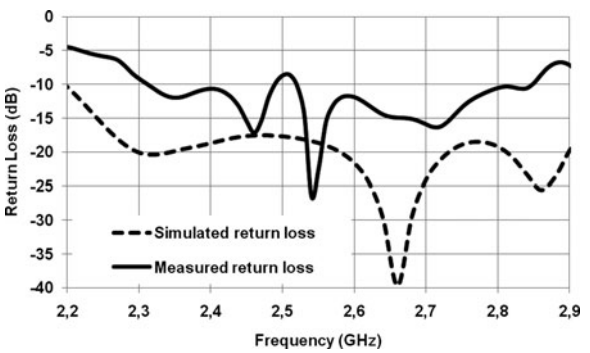

Fig. 7. Simulated and measured reflection coefficient of the antenna.

https://doi.org/10.1017/S1759078712000608 Published online by Cambridge University Press

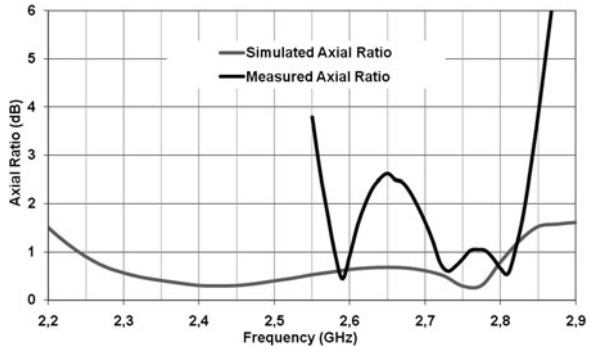

Fig. 8. Simulated and measured boresight AR.

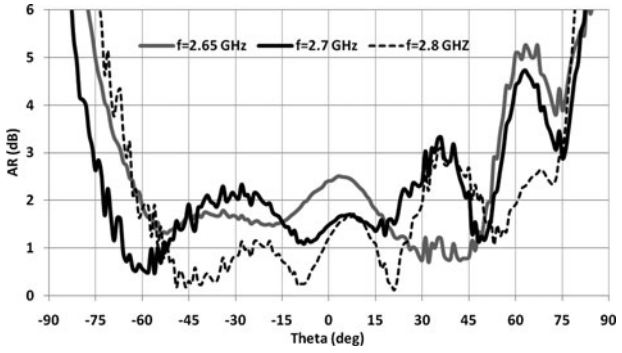

Fig. 10. Measured AR at three frequencies in yz plane ($\varphi = 90^\circ$).

S-parameters exists which also leads to the observed discrepancy in Fig. 8. It should be noted that it is unable to do a probe test for the feeding circuit due to the inconsistency between the probe pads and the circuit lines. A probe circuit test can verify the correct weightings at the output feeding circuit when the whole antenna is assembled.

The AR at 2.7 GHz in two cut planes is shown in Fig. 9. It can be seen that the AR is lower than 3 dB in the $\pm 55^\circ$ conical space region. The antenna has a wide angle scan leading to an important isolation between left and right polarization.

Slight symmetry with respect to the broadside axis of the antenna is observed on the AR. It should be stressed that the feeding cable is plugged into port 1 and two 50 Ω loads are also plugged into ports 6 and 7. The feeding cable and loads are in the azimuth plane. Moreover, a metallic maintaining ring (holding structure) is placed behind the feeding circuit and is used as a transition between the antenna and the rotor in the anechoic chamber. All these leads to a parasitic radiation and goes to asymmetry, even ripples, on the AR radiation patterns. We note that the metallic maintaining structure is not considered in the simulations.

It would be useful to consider the AR s at three frequencies as shown in Fig. 10.

It is undoubtedly true that the circular polarization aperture is wide and exceeds $\pm 55^\circ$ at these three frequencies where the experimental |AR| is below 3 dB. This leads to at least 6% of frequency bandwidth with wide angle circular polarization.

D) Gain and radiation patterns

The measured radiation patterns of the antenna in the xz plane at two frequencies are illustrated in Fig. 11.

The radiation patterns remain almost unchanged over the entire frequency band. The beamwidth angle of the left hand circular polarization (LHCP) radiation patterns decreases slightly as the frequency increases. The isolation between the left and the right components remains lower than -13 dB in the $\pm 60^\circ$ conical space region. Ripples appear also in the radiation patterns due to the scattering fields on the feeding cable, matched loads and the metallic maintaining ring.

As regards the antenna gain and from Fig. 12, the measured directivity remains above 8 dBic and similar to the simulated one. The directivity is calculated by triple integration of the measured radiation patterns in sufficient number of cutting planes [6].

The measured realized gain of the left polarization component remains higher than 2 dBic over (2.52–2.87 GHz) frequency band where the simulated realized gain bandwidth is wider. It should be remembered that a gain of 2 dBic is required to establish the link budget between the satellite and the ground base station. The realized gain takes into account all kinds of losses in the antenna and even the orthogonal circular polarization and radome losses.

Experimental results (i.e. radiation patterns, gain, and AR) improve as the capabilities of the multilayer (four and more) fabrication procedure become easier and cheaper. However, it

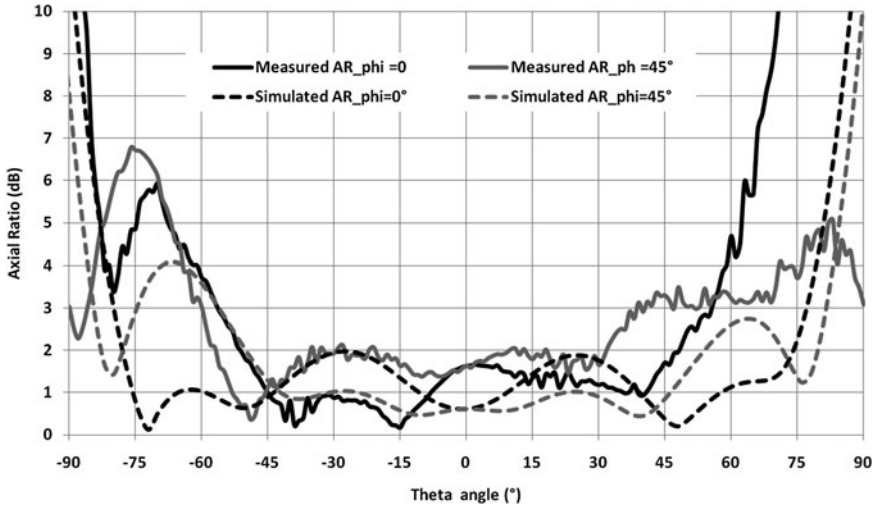

Fig. 9. Measured AR at 2.7 GHz in $\varphi = 0^\circ$ and $\varphi = 45^\circ$ cut planes.

https://doi.org/10.1017/S1759078712000608 Published online by Cambridge University Press

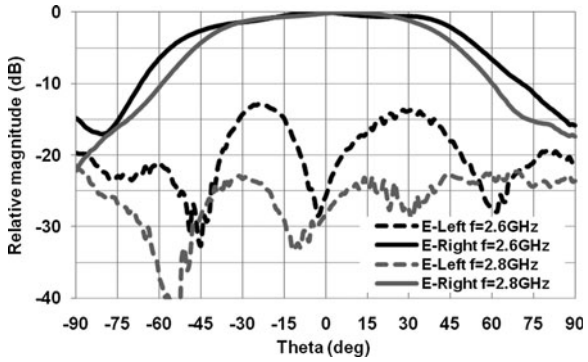

Fig. 11. Measured radiation patterns in *xz* plane at two frequencies.

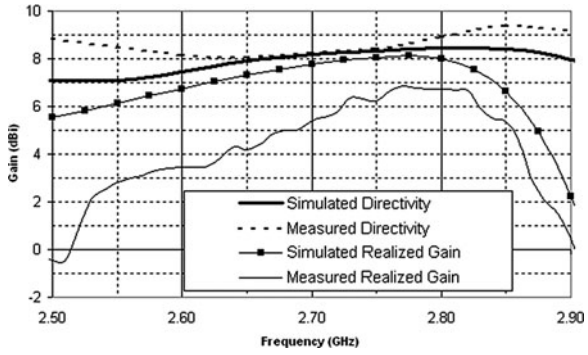

Fig. 12. Measured broadside directivity and IEEE gain versus frequency.

should be also noted that the aluminum support also contributed toward disrupting the radiation patterns.

From all this and despite the air gap present around the two faces of the Rohacell layer and its curvature, it follows that this antenna design provides high quality circular-polarization properties over a wide frequency bandwidth and even far away from the broadside direction.

V. CONCLUSION

A telemetry antenna system intended for agile small satellites is presented and the results are shown and discussed. It provides a simulated AR lower than 3 dB over $\pm 60^{\circ}$ conical space angle and 20% of bandwidth versus $\pm 55^{\circ}$and 6%, respectively for the measured results. There is an experimental operating bandwidth decrease compared with the simulated one due to uncertainly permittivities and faulty assembly leading to an air gap. Therefore, this design provides suitable quality circular-polarization properties for small satellites without having to suspend their mission to download their data and also without sacrificing the antenna's low profile and wide bandwidth. It should be noted that the backward radiation is about -25 dB which will delimit the surface currents on the satellite surfaces.

ACKNOWLEDGEMENT

The authors would like to thank Mr. T. KOLECK from CNES (Centre National d'Etudes Spatiales) – France for valuable suggestions and project management.

REFERENCES

[1] Peragin, E.: Agile satellite with distributed transmission antennas. European patent office, patent number: 09157532.4, October 2009.

[2] Kot, J.S.; Nikolic, N.; Sevimli, O.: An integrated wideband circularly-polarized 60 GHz array antenna with low axial-ratio, in The 2nd Int. Conf. on Wireless Broadband and Ultra Wideband Communications, (AusWireless 2007), IEEE Computer Society.

[3] Nasimuddin, A.; Yong, Y.; Chen, Z.N.; Alphones, A.: Circularly polarized F-slot microstrip antenna with wide beamwidth, in European Microwave Conf., Rome, Italy, October 2009, 1531–1534.

[4] Mak, K.M.; Luk, K.M.: A circularly polarized antenna with wide axial ratio beamwidth. IEEE Trans. Antennas Propag., **57** (10, Part: 2) (2009), 3309–3312.

[5] Croq, F.; Pozar, D.: Millimeter-wave design of wide-band aperture coupled stacked microstrip antennas. IEEE Trans. Antennas Propag., **39** (1991), 1770–1776.

[6] Hollis, J.S.; Lyon, T.J.; Clayton, L. Jr.: Eds., Microwave Antennas Measurements, Scientific Atlanta, Atlanta, GA, USA, 1970.

Majed Koubeissi was born in Saida, Lebanon, on December 24, 1979. He received the B.S. degree in Telecommunication and Networks from Lebanese University, Saida, Lebanon, in 2001 and the degree of High Frequency Electronics Engineering from the ENSIL School, Limoges, France in 2004. He received the Ph.D. degree in Telecommunication from the XLIM Research Laboratory, University of Limoges, France in 2007. Since 2007, he has been an R&D engineer at the Wave and Associated Systems Department of the XLIM Research Laboratory. His research interests include phased arrays, beamforming networks, multiband antennas, DRAs, and circular polarized antennas.

Eric Arnaud was born in France in 1970. He received the Diplôme D'Etudes Supérieures Specialisées (DESS) and Ph.D. degrees in Electronics and Telecommunication from the University of LIMOGES in 1994 and 2010, respectively. He did his Ph.D. on circularly polarized EBG antenna. From 1996 to 2001, he has been in charge of the Microwave part of Free-Electron Laser (L.U.R.E). Since 2001, he has been in charge of XLIM laboratory's antenna test range. He participated in several research projects related to the design, development and characterization of antennas. His research interests are mainly in the fields of circularly polarized EBG antenna and realization of antennas through ink-jetting of conductive inks on RF substrates.

https://doi.org/10.1017/S1759078712000608 Published online by Cambridge University Press

Marc Thevenot was born in Limoges, France, in February 1971. He received the B.S. and M.Sc. degrees in Microwaves and Doctor's degree in Electronics from the University of Limoges, Limoges, France, in 1995, 1995, and 1999, respectively. In 2001, he joined the National de la Recherche Scientifique (CNRS), Limoges, France. His current research interest is microwave electromagnetism applied to the antenna domain and electromagnetic bandgap (EBG) materials for microwaves.

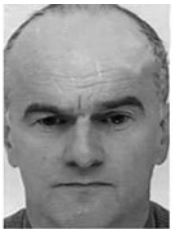

Thierry Monediere was born in 1964 in Tulle (France). He obtained his Ph.D. in 1990 in the IRCOM Laboratory of the University of Limoges. He is actually Professor in the University of Limoges and develops his research activities in the XLIM Laboratory (UMR CNRS/University of Limoges). He works on multifunctional antennas, EBG antennas, and also active antennas

Hubert Diez was born in Oran (France) in 1957. He is a graduate from Limoges University (1981) and a post-graduate from Toulouse University (1985, telecommunications, microwaves + antennas speciality). He started his career in 1981, in Thomson-CSF as an engineer in the field of space telecommunications, and more particularly in technical design and development activities, in the fields of radio transmission, ultra-high frequencies, and antenna for space applications (space segment). In 1986, he joined the CNES Toulouse Space Centre to develop antenna modelization activities for French civil and military programs. In 1996, he joined the Programme Directorate, where he was responsible for wide band services applications, before managing in 2004 the Telecom Applications and Ground Segment Department. From 2007, until now he is the head of the CNES antenna section. He has 14 patents and is the author of more than 50 international papers.

Eric Peragin is a TT&C expert in the CNES Transmission Techniques and Signal Processing Department, having worked in this area for more than 20 years. He designed the high-performance Rx/Tx used on board the Myriade microsatellite family, also used for the intersatellite link of cometarian probes Rosetta (ESA/CNES/DLR) and Deep Impact (NASA). He participated in the development of Mars Data Relay equipment for Mars 96, Mars Observer, and Mars Global Surveyor missions. He is now responsible for the development of CNES new generation high-performance equipment for micro satellites and CubeSats in S and X bands.

https://doi.org/10.1017/S1759078712000608 Published online by Cambridge University Press